Synthesis and gas transport properties of new polynorbornene dicarboximides bearing trifluoromethyl isomer moieties

Jorge A Cruz-Morales[1], Joel Vargas[2], Arlette A Santiago[3], Salomón R Vásquez-García[3], Mikhail A Tlenkopatchev[1], Tomás de Lys[4] and Mar López-González[4]

Abstract

This work reports on the synthesis and ring-opening metathesis polymerization (ROMP) of new structural isomers based on norbornene dicarboximides bearing trifluoromethyl moieties, specifically, N-2-trifluoromethylphenyl-*exo-endo*-norbornene-5,6-dicarboximide (**2a**) and N-3-trifluoromethylphenyl-*exo-endo*-norbornene-5,6-dicarboximide (**2b**) using tricyclohexylphosphine [1,3-bis(2,4,6-trimethylphenyl)-4,5-dihydroimidazol-2-ylidene][benzylidene] ruthenium dichloride (**I**), bis(tricyclohexylphosphine) benzylidene ruthenium (IV) dichloride (**II**), and bis(tricyclohexylphosphine) *p*-fluorophenylvinylidene ruthenium (II) dichloride (**III**). It is observed that the $-CF_3$ moiety attached to the *ortho* position of the aromatic ring increases the thermal and mechanical properties of the polymer, whereas the *meta* substitution has the opposite effect. A comparative study of gas transport in membranes based on these fluorinated polynorbornenes showed that the $-CF_3$ *ortho* substitution increases the permeability of the polymer membrane as a consequence of the increase of both the gas solubility and the gas diffusion. In contrast, the gas permeability coefficients of the *meta*-substituted polymer membrane are rather similar to those of the non-fluorinated one attributed to a lower fractional free volume. The *meta*-substituted polymer membrane besides showing the largest permselectivity coefficients of all the isomers studied here was also found to have one of the largest permselectivity coefficients reported to date for separating hydrogen/propylene in glassy polynorbornene dicarboximides.

Keywords

Structural isomers, ROMP, polynorbornene dicarboximide, gas transport

Introduction

The ever increasing development of new advanced materials for specific applications has encouraged several studies about the effect of the positional isomers on the optical, electrochemical, and photovoltaic properties of their corresponding polymers, among others.[1–3] In the membrane science and technology field, structural isomers have been used as a suitable approach to produce polymer membranes with enhanced gas permeability and selectivity by adopting specific polymer structures for tuning the cavity sizes and distributions.[4] For instance, thermally rearranged polybenzoxazole membranes derived from polyhydroxylamides bearing a *para* linkage in the backbone skeleton showed relatively high gas permeability values with lower gas permselectivity compared to those membranes with the

[1] Instituto de Investigaciones en Materiales, Universidad Nacional Autónoma de México, Apartado Postal 70-360, CU, Coyoacán, México DF 04510, México.
[2] Instituto de Investigaciones en Materiales, Unidad Morelia, Universidad Nacional Autónoma de México, Antigua Carretera a Pátzcuaro No. 8701, Col. Ex Hacienda de San José de la Huerta, C.P. 58190, Morelia, Michoacán, México.
[3] Facultad de Ingeniería Química, Universidad Michoacana de San Nicolás de Hidalgo, Morelia, Michoacán, C.P. 58060, México.
[4] Instituto de Ciencia y Tecnología de Polímeros (ICTP-CSIC), Juan de la Cierva, 3, Madrid 28006, Spain.

Corresponding authors:
Mikhail A Tlenkopatchev, Instituto de Investigaciones en Materiales, Universidad Nacional Autónoma de México, Apartado Postal 70-360, CU, Coyoacán, México DF 04510, México.
Email: tma@unam.mx
Mar López-González, Instituto de Ciencia y Tecnología de Polímeros (ICTP-CSIC), Juan de la Cierva, 3, Madrid 28006, Spain.
Email: mar@ictp.csic.es

meta linkage, indicating that the difference in the polymer chain structure between *para* and *meta* linkages changed the chain packing.[5,6] Taking into account that the ring-opening metathesis polymerization (ROMP) is a very important tool for synthesizing macromolecular architectures which can undergo further functionalization, fluorine-containing norbornene monomers have been gathering much attention since the functional and high-performance polymers derived from them exhibit suitable thermomechanical and chemical properties that allow potential applications as gas separation membranes.[7–9]

Furthermore, fluorinated norbornene monomers can be easily modified, thus facilitating the way to prepare homologous functionalized series of norbornene isomers. In this regard, the combination study on positional isomeric effect of fluorinated moieties and the gas transport in membranes derived from these ROMP-prepared polymers is of great importance in understanding the relationship between their structure and intrinsic properties. Thus, we recently reported the hydrogenation of high-molecular-weight fluorine-containing polynorbornene dicarboximides by two approaches.[10] A comparative study of gas transport in membranes based on these hydrogenated polynorbornenes as well as in their unsaturated analogues revealed that after the hydrogenation of the backbone double bonds of the polymer, the gas permselectivity of the membranes is enhanced as a consequence of the increase of both the gas diffusivity selectivity and the gas solubility selectivity.

In our quest to elucidate how slight modifications in the chemical structure, such as substitution at the *ortho*, *meta*, and *para* positions of the phenyl ring, affect the gas transport properties of functionalized polynorbornene membranes, in this work, we extended the preceding studies to the synthesis and further ROMP process of new structural isomers based on norbornene dicarboximides bearing aromatic trifluoromethyl moieties, along with the investigation of the gas transport properties in the membranes obtained from these macromolecules. Likewise, the thermomechanical properties, together with the structural and physical properties of the formed polymers, are also studied.

Experimental part

Techniques

Proton (^{1}H), carbon 13 (^{13}C), and fluorine 19 (^{19}F) nuclear magnetic resonance (NMR) spectra were recorded on a Varian spectrometer (Palo Alto, California, USA) at 300, 75, and 300 MHz, respectively, in deuterated chloroform (CDCl$_3$). Tetramethylsilane (TMS) and trifluoroacetic acid (TFA) were used as internal standards, respectively. Glass transition temperatures (T_gs) were determined in a DSC-7 calorimeter (Perkin Elmer Inc., Waltham, Massachusetts, USA) at a scanning rate of 10°C min^{-1} under nitrogen (N$_2$)

atmosphere. The samples were encapsulated in standard aluminum differential scanning calorimeter (DSC) pans. Each sample was run twice on the temperature range between 30°C and 300°C under N$_2$ atmosphere. The T_g values were determined graphically from the heat flow temperature curve as the cut point between the line extrapolated from the vitreous area and the bisector of the transition traced by its midpoint, that is, the corresponding temperature to the half of the increase in specific heat in the thermogram. The T_g values obtained were confirmed by Thermomechanical analysis (TMA) from the first heating cycle conducted at a rate of 10°C min^{-1} under N$_2$ atmosphere using a thermomechanical analyzer (model TMA 2940, TA Instruments, New Castle, Delaware, USA). The T_g values were also determined graphically from the dimensional change–temperature curve and assigned by the first inflection point of the trace in the intersection of the tangents drawn at the onset and the end point temperature of this transition. Onset decomposition temperature (T_d) was determined using thermogravimetric analysis (TGA), which was performed at a heating rate of 10°C min^{-1} under N$_2$ atmosphere with a DuPont 2100 instrument. The decomposition temperatures were determined from the weight loss temperature curve in a similar way to the one used for the TMA. Mechanical properties under tension, Young's modulus (E) and tensile strength (σ_u), were measured in an Instron universal mechanical testing machine (model 1125-5500R, Norwood, Massachusetts, USA) using a 50-kg cell at a crosshead speed of 10 mm min^{-1} according to the ASTM D1708 standard in film samples of 0.5 mm of thickness at room temperature. Molecular weights and molecular weight distributions were determined with reference to polystyrene standards on a Waters 2695 Alliance gel permeation chromatography (GPC) at 35°C in tetrahydrofuran using a universal column and a flow rate of 0.5 mL min^{-1}. Wide-angle X-ray diffraction (WAXD) measurements of the as-cast polymer films were carried out in a Siemens D-5000 diffractometer between 4° and 70° 2θ at 35 kV, 25 mA, using copper K_α radiation (1.54 Å). Tapping mode atomic force microscopy (TM-AFM) was performed in air atmosphere using a scanning probe microscope (JSPM-4210, JEOL, Japan), with an NSC12 µmasch needle (an ultrasharp silicon probe cantilever provided by the company MikroMasch, San Jose, California, USA). The samples were imaged at ambient conditions.

Reagents

Exo (90%)–*endo* (10%) monomer mixture of norbornene-5,6-dicarboxylic anhydride (NDA) was prepared via Diels–Alder condensation of cyclopentadiene and maleic anhydride according to literature.[11] 2-(Trifluoromethyl)aniline, 3-(trifluoromethyl)aniline, and 4-(trifluoromethyl)aniline were purchased from Aldrich Chemical Co. (St Louis, Missouri, USA) and used without further purification.
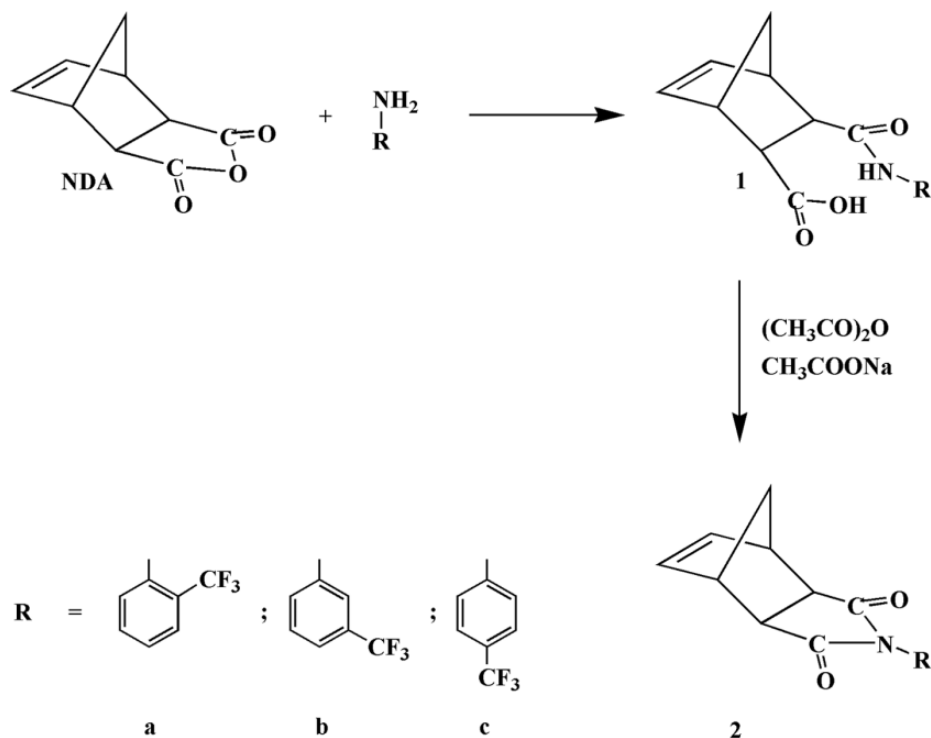
Figure 1. Synthesis of fluorine-containing norbornene dicarboximide structural isomers.

1,2-Dichloroethane, chlorobenzene, and dichloromethane were dried over anhydrous calcium chloride and distilled over calcium hydride. Tricyclohexylphosphine [1,3-bis (2,4,6-trimethylphenyl)-4,5-dihydroimidazol-2-ylidene] [benzylidene] ruthenium dichloride (**I**) and bis(tricyclohexylphosphine) benzylidene ruthenium (IV) dichloride (**II**) were purchased from Aldrich Chemical Co. and used as received. Bis(tricyclohexylphosphine) *p*-fluorophenylvinylidene ruthenium (II) dichloride (**III**) was prepared according to literature.[12]

Synthesis of monomers

Synthesis and characterization of monomer N-2-trifluoromethylphenyl-norbornene-5,6-dicarboximide (2a).
NDA (5 g, 30.5 mmol) was dissolved in 50 mL dichloromethane. An amount of 4.9 g (30.4 mmol) of 2-(trifluoromethyl)aniline in 5 mL dichloromethane is added dropwise to the stirred solution of NDA. The reaction was maintained at reflux for 5 h and then cooled to room temperature. The precipitate was recovered by filtration and dried to give 8.8 g of amic acid (**1a**). The obtained amic acid (**1a**; 8.8 g, 27.0 mmol), anhydrous sodium acetate (1.1 g, 13.6 mmol), and acetic anhydride (12.0 g, 117 mmol) were heated at 70–80°C for 12 h and then cooled. The solid which is crystallized out on cooling was filtered, washed several times with cold water, and dried in a vacuum oven at 50°C overnight. A mixture of *exo* (90%) and *endo* (10%) monomers **2a** (Figure 1) was obtained after two

recrystallizations from ethanol: yield = 87%. Melting point (m.p.) = 208–209°C.

Fourier transform infrared (FTIR): ν 3071 (C=C–H aromatic (ar.) stretching (str.)), 2973 (C–H asymmetric (asym.) str.), 2943, 2877 (C–H symmetric (sym.) str.), 1774 (C=O), 1712 (C=O), 1605, 1500 (C=C str.), 1458 (C–H def), 1370 (C–N), 1317 (C–F), 1157, 1058, 875 cm^{-1}.

^{1}H NMR (300 MHz, CDCl$_3$, ppm): δ 7.78 (1H, d), 7.66–7.57 (2H, m), 7.18 (1H, t), 6.33 (2H, s), 3.41 (2H, s), 2.93 (1H, s), 2.86 (1H, s), 1.79–1.51 (2H, m).

^{13}C NMR (75 MHz, CDCl$_3$, ppm): δ 176.7, 138.1, 133.1, 130.9, 130.1, 127.4, 48.7, 48.0, 45.4, 43.1, 42.5.

^{19}F NMR (300 MHz, CDCl$_3$, ppm): δ −60.3, −60.5.

Synthesis and characterization of monomer N-3-trifluoromethylphenyl-norbornene-5,6-dicarboximide (2b).
NDA (5 g, 30.5 mmol) was dissolved in 50 mL dichloromethane. An amount of 4.9 g (30.4 mmol) of 3-(trifluoromethyl)aniline in 5 mL dichloromethane is added dropwise to the stirred solution of NDA. The reaction was maintained at reflux for 2 h and then cooled to room temperature. The precipitate was recovered by filtration and dried to give 9.2 g of amic acid **1b**. The obtained amic acid **1b** (9.2 g, 28.2 mmol), anhydrous sodium acetate (1.1 g, 13.6 mmol), and acetic anhydride (12.0 g, 117 mmol) were heated at 70–80°C for 12 h and then cooled. The solid which is crystallized out on cooling was filtered, washed several times with cold water, and dried in a vacuum oven at 50°C overnight. A mixture of *exo* (90%) and *endo* (10%)

Table 1. Polymerization conditions of fluorine-containing norbornene dicarboximides **2a**, **2b**, and **2c**, respectively.

Entry	Monomer	Catalyst[a]	Temperature (°C)	Time (h)	*Cis* content in polymer (%)[b]	Yield (%)[c]	M_n ($\times 10^{-5}$)[d]	MWD[d]
1	**2a**	**I**	45	2	50	96	2.79	1.22
2	**2a**	**II**	45	2	23	92	2.58	1.14
3	**2a**	**III**	80[e]	12	11	94	2.68	1.18
4	**2b**	**I**	45	2	48	97	2.82	1.25
5	**2b**	**II**	45	2	18	94	2.62	1.12
6	**2b**	**III**	80[e]	12	10	95	2.73	1.19
7	**2c**	**I**	45	2	52	98	2.86	1.28
8	**2c**	**II**	45	2	20	94	2.64	1.11
9	**2c**	**III**	80[e]	12	10	95	2.74	1.20

2a: *N*-2-trifluoromethylphenyl-*exo-endo*-norbornene-5,6-dicarboximide; **2b**: *N*-3-trifluoromethylphenyl-*exo-endo*-norbornene-5,6-dicarboximide; **2c**: *N*-4-trifluoromethylphenyl-norbornene-5,6-dicarboximide; **I**: tricyclohexylphosphine [1,3-bis(2,4,6-trimethylphenyl)-4,5-dihydroimidazol-2-ylidene][benzylidene] ruthenium dichloride; **II**: bis(tricyclohexylphosphine) benzylidene ruthenium (IV) dichloride; **III**: bis(tricyclohexylphosphine) *p*-fluorophenylvinylidene ruthenium (II) dichloride; ¹H NMR: proton nuclear magnetic resonance; GPC: gas permeation chromatography.
[a]Molar ratio of monomer to catalyst = 1000, 1,2-Dichloroethane as solvent, Initial monomer concentration $[M_o]$ = 0.7 mol L^{-1}.
[b]Determined by ¹H NMR.
[c]Methanol insoluble polymer.
[d]GPC analysis in tetrahydrofuran with polystyrene calibration standards.
[e]Chlorobenzene as solvent.

monomers **2b** (Figure 1) was obtained after two recrystallizations from ethanol: yield = 88%. m.p. = 220–221°C.

FTIR: ν 3093 (C=C–H ar. str), 2980 (C–H asym. str.), 2889 (C–H sym. str.), 1772 (C=O), 1698 (C=O), 1609, 1492 (C=C str), 1453 (C–H def), 1382 (C–N), 1323 (C–F), 1164, 1063, 787 cm^{-1}.

¹H NMR (300 MHz, CDCl₃, ppm): δ 7.76–7.49 (4H, m), 6.36 (2H, s), 3.41 (2H, s), 2.88 (2H, s), 1.67–1.45 (2H, m).

¹³C NMR (75 MHz, CDCl₃, ppm): δ 176.5, 137.9, 132.2, 129.6, 125.2, 123.3, 47.8, 45.8, 42.9.

¹⁹F NMR (300 MHz, CDCl₃, ppm): δ −61.9.

Synthesis and characterization of monomer N-4-trifluoromethylphenyl-norbornene-5,6-dicarboximide (2c). NDA (5 g, 30.5 mmol) was dissolved in 50 mL dichloromethane.[13] An amount of 4.9 g (30.4 mmol) of 4-(methyl)aniline in 5 mL of dichloromethane is added dropwise to the stirred solution of NDA. The reaction was maintained at reflux for 2 h and then cooled to room temperature. The precipitate was recovered by filtration and dried to give 9.7 g of amic acid **1c**. The obtained amic acid **1c** (9.7 g, 29.8 mmol), anhydrous sodium acetate (1.1 g, 13.6 mmol), and acetic anhydride (12.0 g, 117 mmol) were heated at 70–80°C for 12 h and then cooled. The solid which is crystallized out on cooling was filtered, washed several times with cold water, and dried in a vacuum oven at 50°C overnight. A mixture of *exo* (90%) and *endo* (10%) monomers **2c** (Figure 1) was obtained after two recrystallizations from ethanol: yield = 91%. m.p. = 181–189°C.

FTIR: ν 3079 (C=C–H ar. str), 2987 (C–H asym. str.), 2887 (C–H sym. str.), 1772 (C=O), 1702 (C=O), 1612, 1517 (C=C str), 1469 (C–H def), 1384 (C–N), 1320 (C–F), 1164, 1062, 788 cm^{-1}.

¹H NMR (300 MHz, CDCl₃, ppm): δ 7.74 (2H, d), 7.47 (2H, d), 6.36 (2H, s), 3.41 (2H, s), 2.88 (2H, s), 1.65–1.44 (2 H, m).

¹³C NMR (75 MHz, CDCl₃, ppm): δ 176.4, 137.9, 134.5, 126.2, 52.2, 47.8, 45.8, 42.9.

¹⁹F NMR (300 MHz, CDCl₃, ppm): δ −62.0.

Metathesis polymerization of monomers

Polymerizations were carried out in glass vials under dry N₂ atmosphere. They were inhibited by adding a small amount of ethyl vinyl ether, and the solutions were poured into an excess of methanol. The polymers were purified by solubilization in chloroform containing a few drops of 1 N hydrochloric acid and precipitation again into methanol. The obtained polymers were dried in a vacuum oven at 40°C to constant weight. The polymerization conditions are collected in Table 1.

Polymerization of 2a. Monomer **2a** (1.0 g, 3.25 mmol) and catalyst **I** (2.76×10^{-3} g, 0.0032 mmol) were stirred in 4.6 mL of 1,2-dichloroethane at 45°C for 2 h (Figure 2). The obtained poly(*N*-2-trifluoromethylphenyl-norbornene-5,6-dicarboximide) (**3a**) was soluble in chloroform and dichloroethane.

FTIR (thin film, cm^{-1}): ν 3014 (C=C–H ar. str), 2926, 2857 (C–H sym. str.), 1783 (C=O), 1712 (C=O), 1608, 1500 (C=C str), 1455, 1373 (C–N), 1314 (C–F), 1275, 1158, 1107, 1060, 762 cm^{-1}.

¹ H NMR (300 MHz, CDCl₃, ppm): δ 7.73–7.44 (3H, m), 7.12 (1H, s), 5.73 (1H, s, *trans*), 5.50 (1H, s, *cis*), 3.14 (2H, s), 2.87 (2H, s), 2.16 (1H, s), 1.65 (1H, s).

¹⁹F NMR (300 MHz, CDCl₃, ref. TFA [−77 ppm], δ, ppm): −60.0, −60.5.

Polymerization of 2b. Monomer **2b** (1.0 g, 3.25 mmol) and catalyst **I** (2.76×10^{-3} g, 0.0032 mmol) were stirred in 4.6 mL 1,2-dichloroethane at 45°C for 2 h (Figure 2). The obtained poly(*N*-3-trifluoromethylphenyl-norbornene-5,6-
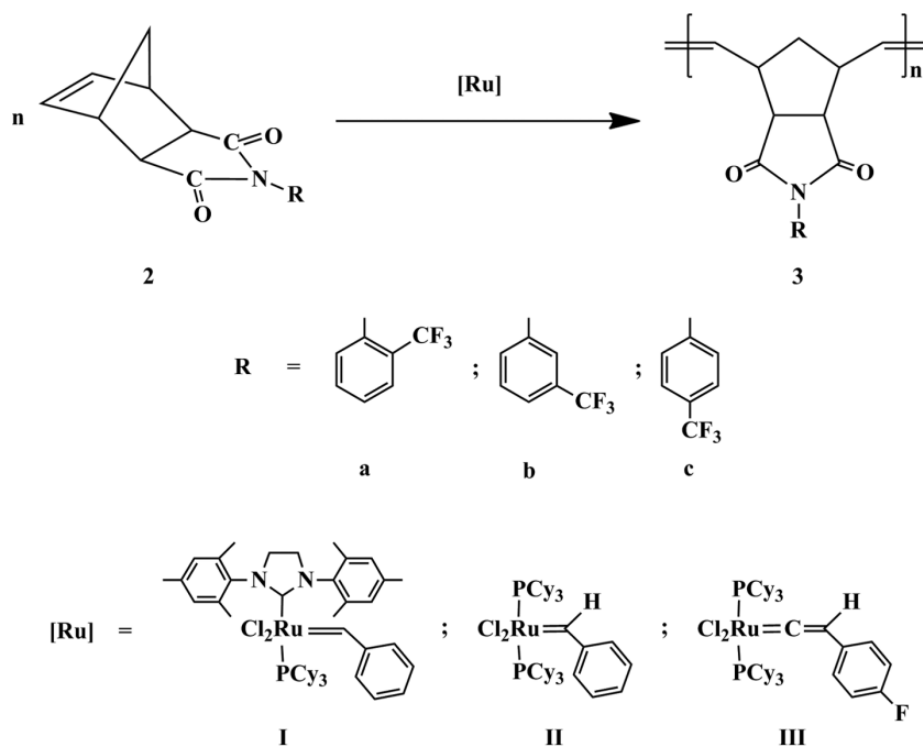
Figure 2. ROMP of norbornene dicarboximide structural isomers bearing trifluoromethyl moieties. ROMP: ring-opening metathesis polymerization.

dicarboximide) (**3b**) was soluble in chloroform and dichloroethane.

FTIR (thin film, cm^{-1}): ν 2949 (C=C–H ar. str), 2861 (C–H sym. str.), 1778 (C=O), 1708 (C=O), 1597, 1494 (C=C str), 1454, 1370 (C–N), 1324 (C–F), 1160, 1118, 1067, 693 cm^{-1}.

^{1}H NMR (300 MHz, CDCl$_3$, ppm): δ 7.61–7.33 (4H, m), 5.80 (1H, s, *trans*), 5.57 (1H, s, *cis*), 3.19 (2H, s), 2.89 (2H, s), 2.19 (1H, s), 1.63 (1H, s).

^{19}F NMR (300 MHz, CDCl$_3$, ref. TFA [−77 ppm], δ, ppm): −61.9.

Polymerization of 2c. Monomer **2c** (1.0 g, 3.25 mmol) and catalyst **I** (2.76 × 10^{-3} g, 0.0032 mmol) were stirred in 4.6 mL 1,2-dichloroethane at 45°C for 2 h (Figure 2).[13] The obtained poly(*N*-4-trifluoromethylphenyl-norbornene-5,6-dicarboximide) (**3c**) was soluble in chloroform and dichloroethane.

FTIR (thin film, cm^{-1}): ν 2955 (C=C–H ar. str), 2859 (C–H sym. str.), 1778 (C=O), 1708 (C=O), 1614, 1519 (C=C str), 1453, 1371 (C–N), 1319 (C–F), 1161, 1108, 1064, 839 cm^{-1}.

^{1}H NMR (300 MHz, CDCl$_3$, ppm): δ 7.72–7.25 (4 H, m), 5.79 (1H, s, *trans*), 5.54 (1H, s, *cis*), 3.15 (2H, s), 2.86 (2H, s), 2.20 (1H, s), 1.65 (1H, s).

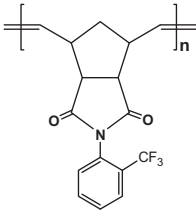^{19}F NMR (300 MHz, CDCl$_3$, ref. TFA [−77 ppm], δ, ppm): −62.1.
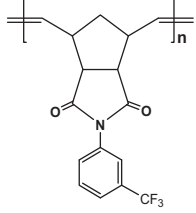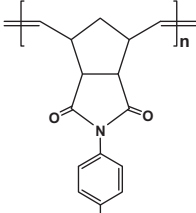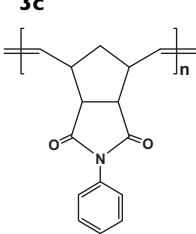
Membranes preparation and permeation experiments

Membranes were cast from polymer solutions in chloroform at room temperature. The density of the membranes was measured at room temperature by the flotation method using ethanol as liquid. The values of the density are shown in Table 2.

Permeation experiments were carried out in a cell made of two semicells separated by the membrane. After making vacuum in the two semicells, gas at a given pressure is introduced into the high pressure or upstream semicell, which is coupled to a Gometrics (Barcelona, Spain) pressure transducer. The gas flowing across the membrane to the low pressure or downstream semicell is monitored as a function of time with an MKS 628/B pressure transducer via a PC. Permeation cell is kept inside a water thermostat at the temperature of interest. If the volume V of the downstream semicell is given in cubic centimeter, the area A of the exposure membrane in square centimeter, its thickness l in centimeter, and the pressure in centimeter mercury (cm Hg), the permeability coefficient P of the gases in the membranes in barrer $\left(1 \text{ barrer} = 10^{-10} \text{cm}^3 (\text{STP}) \text{cm}/(\text{cm}^2 \text{ s cm Hg})\right)$ is given by:

$$P = 3.59 \frac{Vl}{p_0 AT} \lim_{t \to 0} \left(\frac{dp}{dt}\right) \tag{1}$$

Table 2. Physical properties of fluorine-containing polynorbornene dicarboximides obtained using **I**.

Polymer	T_g (°C)	T_d (°C)	σ (MPa)	E (MPa)	ρ (g/mL)	FFV	d_{spacing} (Å)
3a	232	417	57.1	1504	1.405	0.133	4.00
3b	180	415	35.5	1265	1.432	0.116	3.97
3c	222	417	48.1	1307	1.366	0.157	4.10
PPNDI	222	418	57.0	1560	1.170	0.187	—

3a: poly(*N*-2-trifluoromethylphenyl-*exo, endo*-norbornen-5,6-dicarboximide); **3b**: poly(*N*-3-trifluoromethylphenyl-*exo, endo*-norbornen-5,6-dicarboximide); **3c**: poly(*N*-4-trifluoromethylphenyl-*exo, endo*-norbornen-5,6-dicarboximide)[13]; PPNDI: poly(*N*-phenyl-*exo–endo*-norbornen-5,6-dicarboximide)[7]; **I**: tricyclohexylphosphine [1,3-bis(2,4,6-trimethylphenyl)-4,5-dihydroimidazol-2-ylidene][benzylidene] ruthenium dichloride; T_g: glass transition temperature; T_d: onset decomposition temperature; E: Young's modulus; σ: tensile strength.

where T is the absolute temperature and p_0 and p are the upstream and downstream gas pressures, respectively. The p versus t isotherms present a transitory, followed by a straight line ($t \rightarrow \infty$) corresponding to steady-state conditions. The intersection of the straight line with the abscissa axis of the plot is the time lag θ, related to the apparent gas diffusion coefficient by the following equation[14]:

$$D = \frac{l^2}{6\theta}. \qquad (2)$$

The diffusion coefficient (D) is currently given in square centimeter per second units. The apparent solubility coefficient (S) is given by:

$$S = \frac{P}{D}. \qquad (3)$$

The usual units of S are $\text{cm}^3(\text{STP})/(\text{cm}^3 \text{ cm Hg})$.

The gas permeation tests were repeated two to three times at the given conditions, and the averages of the coefficients obtained are reported.

Results and discussion

Monomers **2a**, **2b**, and **2c** were readily prepared in high yields (87–91%). 2-(trifluoromethyl)aniline, 3-(trifluoromethyl)aniline, and 4-(trifluoromethyl)aniline reacted with an *exo* (90%)–*endo* (10%) mixture of norbornene-5,6-dicarboxylic anhydride to the corresponding amic acids, which were cyclized to imides using acetic anhydride as dehydrating agent according to literature (Figure 1).[15,16] ^{1}H, ^{13}C, and ^{19}F NMR spectra confirmed the structures of the monomers. The infrared spectra of the structural isomers showed characteristic peaks around 1778 and 1708 cm^{-1} (asymmetric and symmetric C=O stretching), 1371 cm^{-1} (C–N stretching), 1320 cm^{-1} (C–F stretching). Table 1 summarizes the results of the ROMP of monomers **2a**, **2b**, and **2c** using ruthenium (Ru) catalysts **I**, **II**, and **III**. As it is shown, the mixture of *exo* and *endo* monomers reacted for 2 h giving polymer in high yield (97–99%, entries 1, 4, and 7) when catalysts **I** and **II** were employed. On the other hand, high polymer yields were achieved using catalyst **III** when the polymerization reactions were conducted at 80°C for 12 h (Table 1, entries 3, 6, and 9). This behavior can be explained by the fact that the stronger electron-donating ability of vinylidene group in **III** compared to alkylidene one of the first- and second-generation Grubbs catalyst (**II** and **I**, respectively) can reduce the phosphine dissociation energy and will increase the activation energy of the metathesis reaction. The experimental and theoretical studies clearly indicate that for the Grubbs-type Ru alkylidene complexes, the initiation occurs via dissociative substitution of a phosphine ligand with an olefin substrate resulting in a monoligand complex.[17,18] The computational modeling of Ru alkylidene catalysts revealed that the stability of 14-electron monoligand metal carbenes correlates with the charge at Ru atoms.[19] The more the positive charge, the less stable is since 14-electron Ru is an electron-deficient species. The vinylidene group is notably a better donor than alkylidene one, stabilizing the 14-electron complex **III**.

The results obtained by GPC analysis show that the number-average molecular weights (M_ns) were between 258,000 and 286,000 g mol^{-1}. The experimental M_ns are in agreement with the theoretical ones, however, there are minor differences in the molecular weight of the polymers since the different catalysts lead to different *cis/trans* ratio of the backbone double bonds, and this stereo structure changes the radius of gyration (hydrodynamic volume) at the same molar mass. As shown in Table 1, the molecular weight distribution (MWD) of the polymers **3a**, **3b**, and **3c** obtained using **I** is about $M_w/M_n = 1.22$–1.28, which is broader than polymers prepared using **II** ($M_w/M_n = 1.11$–1.14) and **III** ($M_w/M_n = 1.18$–1.20).

Figures 3 and 4 show the ^{1}H NMR spectra of the fluorinated structural isomers and their corresponding ROMP-prepared polymers using **I**, respectively. As it is observed, the ^{1}H NMR spectra of monomers as well as polymers are quite similar and some slight differences arise in the aromatic proton region due to the position of the fluorinated substituent. In general, the *exo* monomer olefinic signals around $\delta = 6.36$ are replaced by new signals observed around $\delta = 5.79$ and 5.54, which correspond to the *trans* and *cis* double bonds of the polymer main chain. It is important to note that the small peaks at 6.25 ppm correspond to the *endo* monomer olefinic signals from which a content of 10% of this isomer was determined. Since ^{1}H NMR was used to determine the *cis/trans* content in the polymer backbone, from Figure 5, it can be observed that catalyst **I** produced polymers with a mixture of *cis* and *trans* double bonds (48–52% of *cis* structure), whereas catalyst **II** and **III** gave polymers with predominantly *trans* configuration of the double bonds (77–90%).

Changing the position of the –CF$_3$ substituent on the aromatic pendant moiety affects neither the conversion of monomer nor the stereochemistry of the double bonds in the polymer when the same Ru complex is used to polymerize the three fluorinated isomers.

Figure 6 shows the ^{19}F NMR spectra of the polymers **3a**, **3b**, and **3c** prepared by **I**. According to Figure 6, it is appreciated that the *meta* and *para* substitution of the aromatic ring lead to fluorine atoms in **3b** and **3c** that are magnetically equivalent and their signals appear as one peak, around −61.9 ppm and −62.1 ppm, respectively. However, the *ortho* substitution of the aromatic ring in polymer **3a** leads to two inequivalent fluorine atoms that give rise to two signals which are slightly shifted downfield from the position of the *meta*- and *para*-substituted polymers, around −60.0 ppm and −60.5 ppm, respectively. This signal splitting in the ^{19}F NMR spectrum of polymer **3a** could be attributed to different chemical environments resulting from the nearness of the −CF$_3$ group to the imide moiety. It is likely that the bulkiness of the trifluoromethyl group causes that the plane of the aromatic ring be in the plane of symmetry of norbornene generating two preferred and distinct orientations in the *ortho*-substituted phenyl ring that diminish the steric effects. In one orientation, the *ortho* substituent is pointed up, while in the other down. These results are consistent with those reported previously for other polynorbornene derivatives with systematically substituted rings.[20]

The effect that –CF$_3$ group position on the pendant phenyl ring in the polynorbornene dicarboximide had on the physical properties of polynorbornenes with similar structures obtained using **I** is compared in Table 2. As it is observed, the *ortho*-substituted polymer **3a** shows the higher glass transition temperature (T_g), compared to those of the *meta*- and *para*-substituted polymers, which is attributed to an increased hindered rotation of the phenyl group about the C–N bond. The T_gs for *ortho*- and *para*-substituted polymers were observed at 232°C and 222°C, nearly 50°C and 40°C more than the *meta*-substituted polymer **3b**,
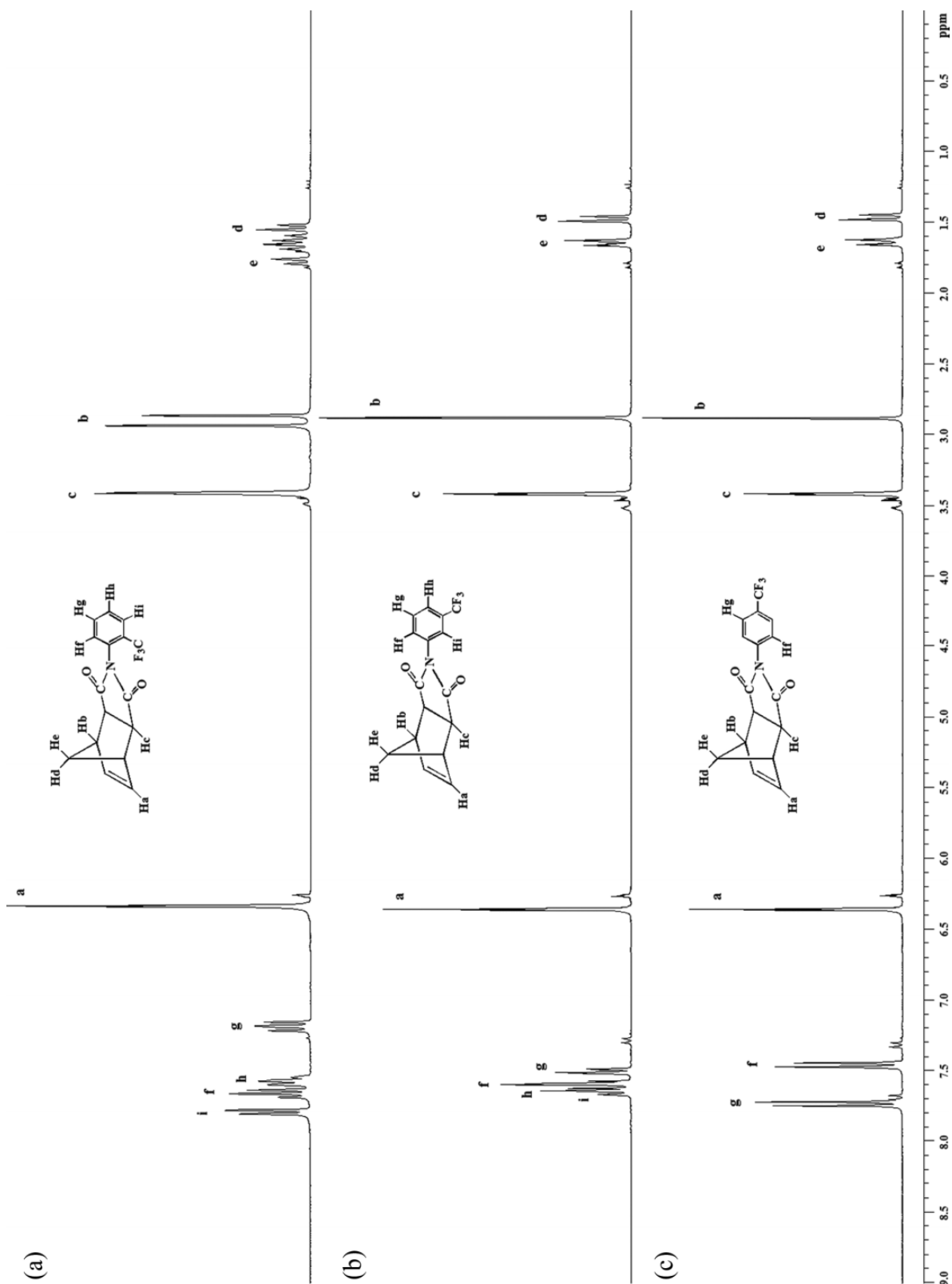
Figure 3. ^{1}H NMR spectra of (a) monomer **2a**, (b) monomer **2b**, and (c) monomer **2c**. ^{1}H NMR: proton nuclear magnetic resonance; **2a**: *N-2-trifluoromethylphenyl-exo-endo-norbornene-5,6-dicarboximide*; **2b**: *N-3-trifluoromethylphenyl-exo-endo-norbornene-5,6-dicarboximide*; **2c**: N-4-trifluoromethylphenyl-norbornene-5,6-dicarboximide.
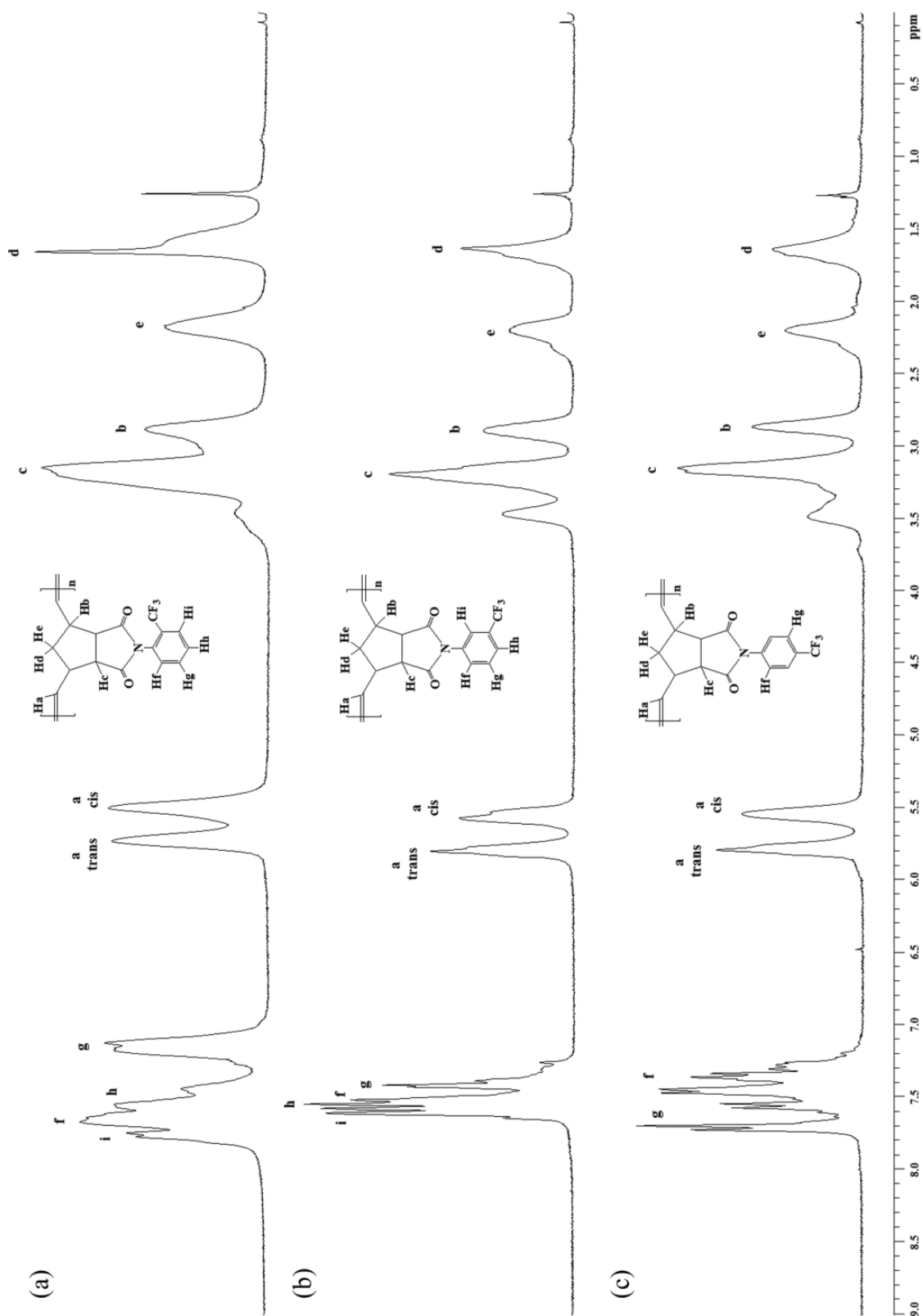
Figure 4. ¹H NMR spectra of (a) polymer **3a**, (b) polymer **3b** and (c) polymer **3c** obtained using **I**. ¹H NMR: proton nuclear magnetic resonance; **3a**: poly(N-2-trifluoromethylphenyl-norbornene-5,6-dicarboximide); **3b**: poly(N-3-trifluoromethylphenyl-norbornene-5,6-dicarboximide); **3c**: poly(N-4-trifluoromethylphenyl-norbornene-5,6-dicarboximide); **I**: tricyclohexylphosphine [1,3-bis(2,4,6-trimethylphenyl)-4,5-dihydroimidazol-2-ylidene][benzylidene] ruthenium dichloride.
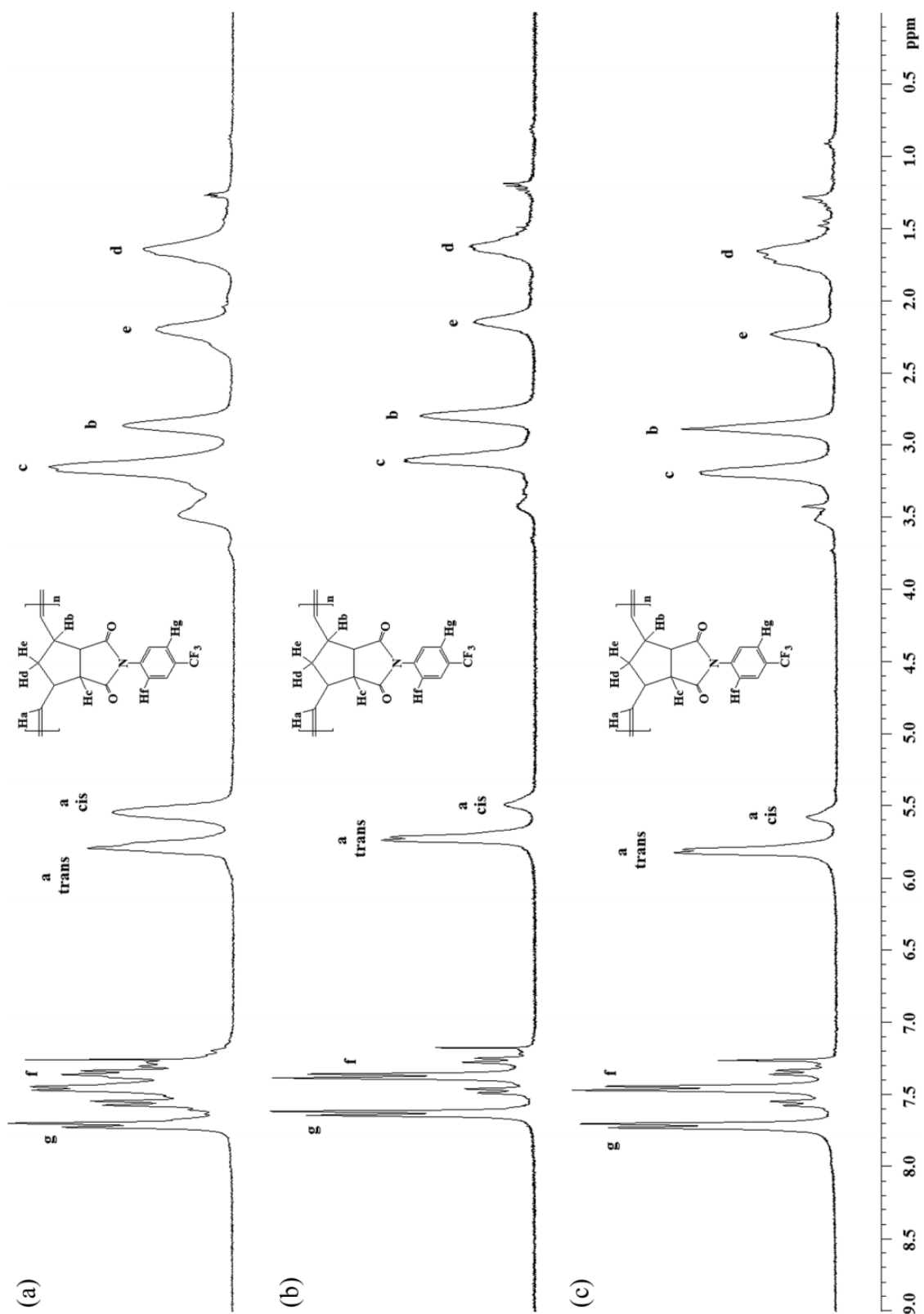
Figure 5. ¹H NMR spectra of polymer **3c** obtained using (a) catalyst **I**, (b) catalyst **II** and (c) catalyst **III**, respectively. ¹H NMR: proton nuclear magnetic resonance.
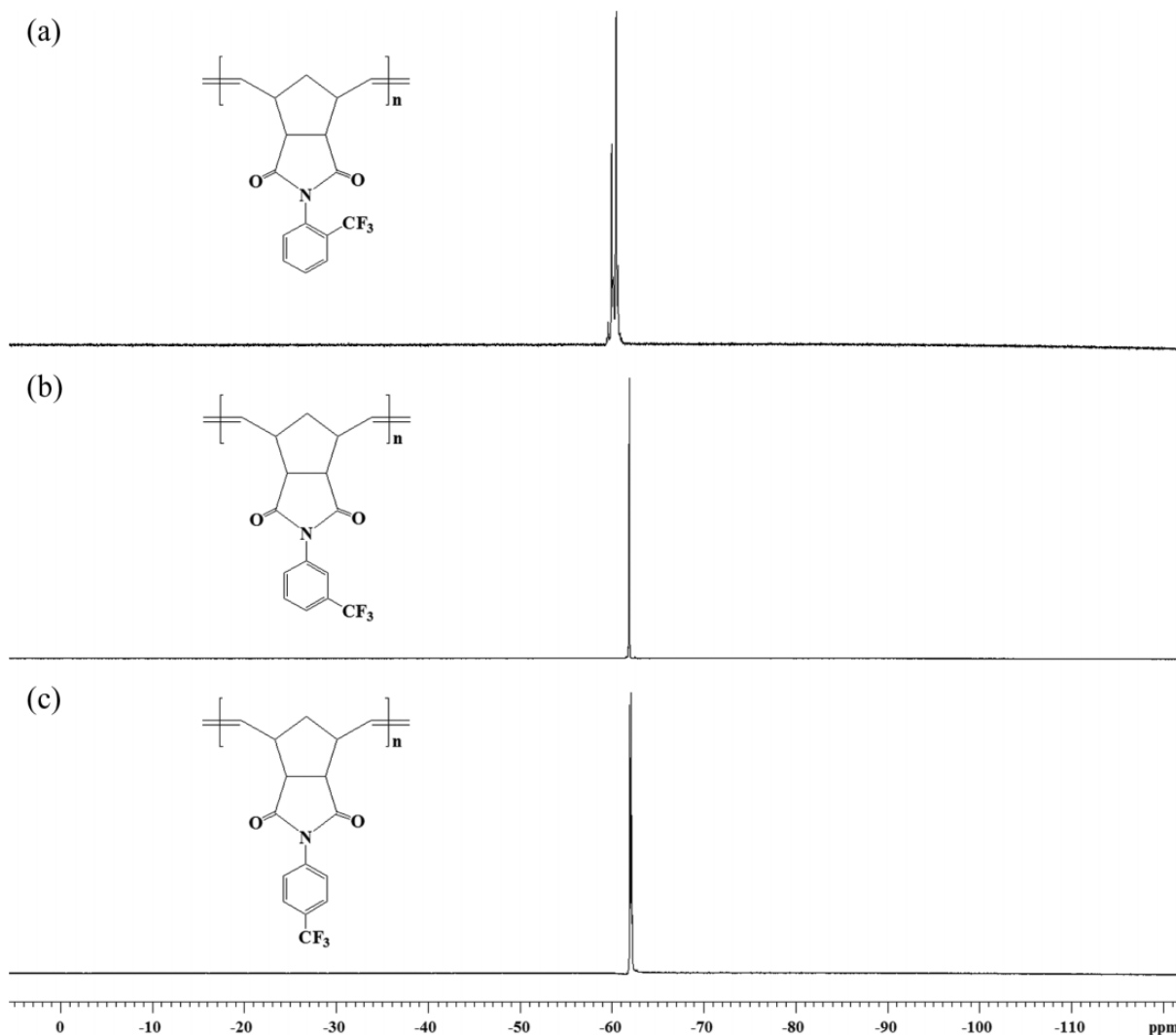
Figure 6. ^{19}F NMR spectra of (a) polymer **3a**, (b) polymer **3b** and (c) polymer **3c** obtained using **I**. ^{19}F NMR: fluorine 19 nuclear magnetic resonance.

respectively. These results, obtained by DSC and confirmed by TMA (Figure 7), indicate that the *ortho* and *para* substitutions lead to restriction in the segmental motion of the polymer backbones.

On the contrary, the *meta* substitution leads to the highest conformational mobility of the polymer chains which in turn is reflected in the lowest T_g of all the polymers obtained (180°C), thus it is worth noting that the T_gs values follow the trend T_g (*ortho*-CF$_3$) > T_g (*para*-CF$_3$) > T_g (*meta*-CF$_3$). Moreover, the T_g for the *para*-substituted polymer **3c** is indistinguishable from that of the unsubstituted polymer poly(*N*-phenyl-*exo-endo*-norbornene-5,6-dicarboximide) (PPNDI), and the value for the *meta*-substituted polymer **3b** is shifted to lower temperature while that for the *ortho*-substituted polymer **3a** is shifted to higher temperature relative to the parent unsubstituted polymer PPNDI.[7] The trends observed for these trifluoromethyl-substituted polynorbornene dicarboximides are consistent

with those previously reported for *ortho*-, *meta*-, and *para*-substituted polynorbornene derivatives.[20,21] The thermal stability of the polymers was studied by TGA under N$_2$ atmosphere. The onset temperature for decomposition of all the polynorbornene dicarboximides studied here are in the range of 415–417°C, which indicate that these regioisomers bearing –CF$_3$ moieties yield polymers of relatively high thermal stability.

The stress–strain measurements in tension for the films of the synthesized polymers indicate that the *ortho*-substituted polymer **3a** exhibits the higher elastic modulus and tensile strength ($E = 1504$ MPa and $\sigma_u = 57.1$ MPa) in comparison with the polymers **3b** and **3c**. This fact also suggests that the presence of the bulky –CF$_3$ moiety pending at the *ortho* position of the phenyl ring in **3a** restricts the ability to attain the relaxation process. On the other hand, the ability of the polymer chains to adopt different conformations in the backbone of the *meta*-substituted polymer
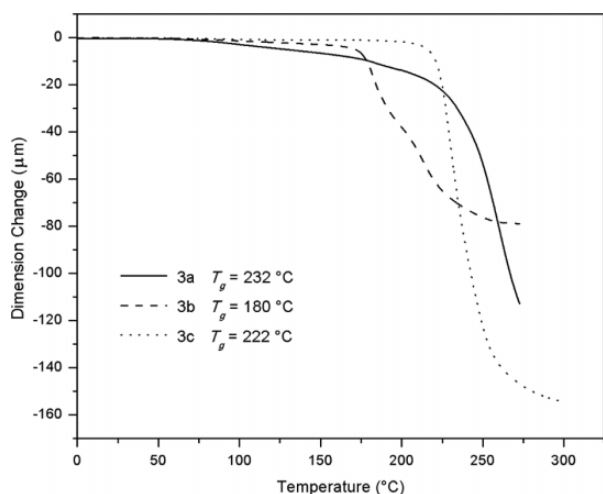
Figure 7. Thermomechanical curves of polymers **3a** (solid line), **3b** (dashed line) and **3c** (dotted line) obtained using **I**.

3b was also reflected in a lesser elastic modulus and tensile strength (E = 1265 MPa and σ_u = 35.5 MPa) as compared to the other CF$_3$-substituted isomers as well as its parent unsubstituted polymer PPNDI, respectively.

The density (ρ) of the membranes was measured at room temperature by the flotation method using ethanol as liquid. Density measurements reported in Table 2 show that the *meta* position of the –CF$_3$ substituent on the aromatic pendant moiety of the polynorbornene dicarboximide **3b** promotes chain packaging efficiency, which is reflected in a higher density value and a lower fractional free volume (FFV), as compared to those of the *ortho*- and *para*-substituted polymers. The FFV was calculated by the Bondi group contribution method[22] from the following equation:

$$\text{FFV} = \frac{(V - V_0)}{V}, \qquad (4)$$

where V is the specific volume $(1/\rho)$, V_0 is the specific occupied volume which according to Bondi's method can be calculated from the van der Waals volume V_w as $V_0 = 1.3 \, V_w$ estimated using van Krevelen's data.[23]
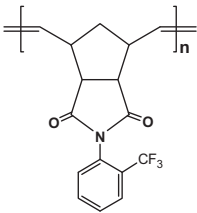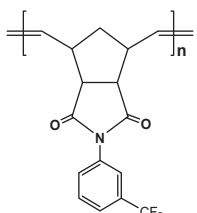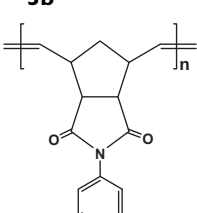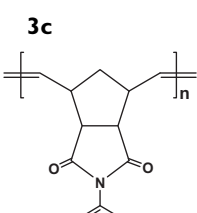
WAXD measurements of the as-cast CF$_3$-substituted polymer films show typical polynorbornene dicarboximide patterns with one broad diffraction peak with a maximum around $2\theta = 20°$.[8,24] The latter evidences that all these polymers as cast are amorphous since no crystallinity was detected either by WAXD or in the thermal measurements described previously. A measure of their mean intersegmental distance or chain packing density could be obtained from the *d*-spacing value at the angle of maximum reflective intensity in the amorphous trace using Bragg's equation, $n\lambda = 2d \sin\theta$.[25] As shown in Table 2, the values of the average *d*-spacing correlate fairly good with those of the FFV, which is considered a measure of the *d*-spacing parameter.

Values of the permeability (P), diffusion (D), and apparent solubility coefficients, at 30°C and 1 atm of pressure, for several gases in the membranes of **3a**, **3b**, and **3c**, obtained using **I**, are shown in Table 3. In the same table and for comparative purposes, the values of these coefficients for the parent unsubstituted PPNDI, reported earlier,[7] are also shown.

In Figure 8, the surface morphologies of (a) *ortho*-substituted polymer **3a**, (b) *meta*-substituted polymer **3b**, and (c) *para*-substituted polymer **3c**, obtained using **I**, are observed by TM-AFM in three dimensions. The surface morphology in (a) shows an uneven architecture characterized by numerous protuberances per unit area that could be attributed to a more restricted side chain mobility that resulted from the steric hindrance of the –CF$_3$ groups in *ortho* position, thus preventing the segmental relaxation of the polymer chain and the –CF$_3$ groups aggregation. In contrast, polymer **3b** seems to have a smooth and more uniform surface morphology that suggests an increased side chain flexibility leading to a higher ability of this polymer to chain packing, which in turn is reflected in the highest density and therefore the lowest FFV of all the polymers discussed here. Finally, the –CF$_3$ substitution in *para* position may strongly increase the ability of the phenyl rings to undergo segmental rotation resulting in a greater tendency for the polymer chains to pack less efficiently. Thus, in (c) a much more disrupted surface morphology is observed, and it could be attributed to a most efficient distortion of the polymer chain packing as a result of the symmetry of the side moiety with the –CF$_3$ groups located at the *para* position. That is, placing the –CF$_3$ substituent symmetrically on the aromatic ring stiffens the chain backbone and increases the FFV of the polymer. In this regard, **3c** exhibits the lowest density and therefore the highest FFV of all the polymers studied.

In general, the permeability coefficients in the structural isomers follow the trends $P(\text{H}_2) > P(\text{CO}_2) > P(\text{O}_2) > P(\text{C}_2\text{H}_4) > P(\text{CH}_4) > P(\text{N}_2) > P(\text{C}_3\text{H}_6)$ that differ from those for the diffusion coefficient which decrease in the order $D(\text{H}_2) > D(\text{O}_2) > D(\text{N}_2) > D(\text{CO}_2) > D(\text{CH}_4) > D(\text{C}_2\text{H}_4) > D(\text{C}_3\text{H}_6)$. Evidently carbon dioxide (CO$_2$) and the most condensable hydrocarbon gases exhibit the larger apparent solubility coefficients (S), obtained from the ratio P/D, in such a way that $S(\text{C}_3\text{H}_6) > S(\text{CO}_2) > S(\text{C}_2\text{H}_4) > S(\text{CH}_4) > S(\text{O}_2) > S(\text{N}_2) > S(\text{H}_2)$. From Table 3, it is seen that the presence of the –CF$_3$ group increases the apparent solubility coefficient in all the structural isomers as compared to those in the non-fluorinated PPNDI membrane. It is well-known that the presence of –CF$_3$ groups produces more sites for gas sorption, thus contributing to higher permeabilities.[26] Moreover, the –CF$_3$ moiety attached to the *ortho* and *para* positions of the phenyl-substituted polymers increases the permeability of the fluorine-containing polynorbornene membranes as reveals the fact that the permeability coefficients of the gases in the fluorinated **3a** and

Table 3. Values of the P, D, and S of different gases.[a]

Polymer	Gas	P (barrers)	D × 10⁸ (cm² s⁻¹)	S × 10³ cm³ cm⁻³ cm Hg
[structure 3a]	H_2	39.25	309.39	1.3
	N_2	1.30	2.83	4.6
	O_2	5.63	7.84	7.2
	CO_2	34.61	2.62	132.1
	CH_4	1.48	0.79	18.7
	C_2H_4	2.45	0.19	126.4
	C_3H_6	1.08	0.033	322.6
3a				
[structure 3b]	H_2	15.10	145.89	1.0
	N_2	0.36	1.37	2.7
	O_2	1.80	3.99	4.5
	CO_2	9.83	0.91	108.5
	CH_4	0.37	0.30	12.3
	C_2H_4	0.55	0.081	67.7
	C_3H_6	0.26	0.014	179.8
3b				
[structure 3c]	H_2	34.42	252.29	1.4
	N_2	1.47	2.78	5.3
	O_2	6.17	8.55	7.2
	CO_2	34.37	2.16	159.5
	CH_4	1.59	0.75	21.0
	C_2H_4	2.40	0.18	133.0
	C_3H_6	1.20	0.041	286.9
3c				
[structure PPNDI]	H_2	11.0	132.0	0.8
	N_2	0.31	2.23	1.4
	O_2	1.44	6.30	2.3
	CO_2	11.44	1.81	63.2
	CH_4	0.54	0.72	7.5
	C_2H_4	0.58	0.30	19.3
	C_3H_6	—	—	—
PPNDI				

[a]The reaction is performed at 30°C and 1 atm upstream pressure in membranes of fluorine-containing polynorbornene dicarboximides obtained using I.
P: permeability; D: diffusion; S: apparent solubility coefficient; H_2: hydrogen; N_2: nitrogen; O_2: oxygen; CO_2: carbon dioxide; CH_4: methane; C_2H_4: ethylene; C_3H_6: propylene; **3a**: poly(N-2-trifluoromethylphenyl-exo–endo-norbornen-5,6-dicarboximide); **3b**: poly(N-3-trifluoromethylphenyl-exo–endo-norbornen-5,6-dicarboximide); **3c**: poly(N-4-trifluoromethylphenyl-exo–endo-norbornen-5,6-dicarboximide)[13]; PPNDI: poly(N-phenyl-exo–endo-norbornen-5,6-dicarboximide)[7]; I: tricyclohexylphosphine [1,3-bis(2,4,6-trimethylphenyl)-4,5-dihydroimidazol-2-ylidene][benzylidene] ruthenium dichloride.

3c membranes are two to three times larger than those in the non-fluorinated PPNDI membrane. This increase in permeability in the fluorinated **3a** and **3c** membranes with regard to that of the non-fluorinated PPNDI membrane arise from both the diffusive process and the gas sorption step. It is worth noting that the latter effect is not observed when the gas permeability coefficients of the *meta*-substituted **3b** membrane are compared to those of the non-fluorinated one. The results show that gas permeability coefficients in both membranes are rather similar as a consequence of the sharp decline of the gas diffusion coefficients in the **3b** membrane, with values ranging from 36% oxygen (O_2) to 73% ethylene (C_2H_4) less than those reported for the PPNDI membrane. The lowering in the diffusion coefficients is mainly due to a lower FFV associated with the higher chain packaging efficiency of this *meta* isomer in comparison with the non-fluorinated as well as the fluorinated polymers, which in turn hinders the diffusion of the gas molecules through the polymer.

The apparent solubility coefficients in the **3b** membrane are also lower than those reported for the membranes of the isomers **3a** and **3c**. In general, gas solubility in glassy polymers is higher than that in rubbery polymers. As it is known, glassy polymers have nonequilibrium excess free volumes, therefore, lower gas solubility can be attributed directly to the less amount of this additional free volume into which sorption can occur.

The dual-mode model, which assumes the glassy state as formed by a continuous phase where microcavities accounting for the excess volume are dispersed, has traditionally been used to interpret gas sorption in glassy polymers. The solubility in the continuous phase obeys Henry's law, while the microcavities act like Langmuir sites in which adsorption processes take place. This Langmuir sorption capacity is often used to correlate the amount of the nonequilibrium excess free volume in the glassy state.[27] The dual-mode model suggests that the Langmuir sorption capacity of glassy membranes depends on $T_g - T$ so that as the polymer T_g decreases, the nonequilibrium excess free volume also decreases at a given temperature T.[28] According to this approach, therefore, the relatively low values of S found for the **3b** membrane used in this study may be due to the nearness of the T_g of the CF_3 *meta*-substituted polymer to the working temperature.

The effect of the position of the $-CF_3$ substituent group on the ring in the performance of polynorbornene dicarboximide membranes was also estimated from the permselectivity coefficient or ideal separation factor of gas A over gas B (α), a measure of the capacity of a polymer membrane to carry out the separation for a given gas pair mixture, given by the following equation:

$$\alpha\left(\frac{A}{B}\right) = \frac{P(A)}{P(B)} = \frac{D(A)}{D(B)} \times \frac{S(A)}{S(B)}. \quad (5)$$

Equation (5), defined as the ratio of pure gas permeability coefficients $P(A)/P(B)$, indicates that the discriminative effects taking place in gas transport in membranes may be governed by the diffusive step, the solubility process, or
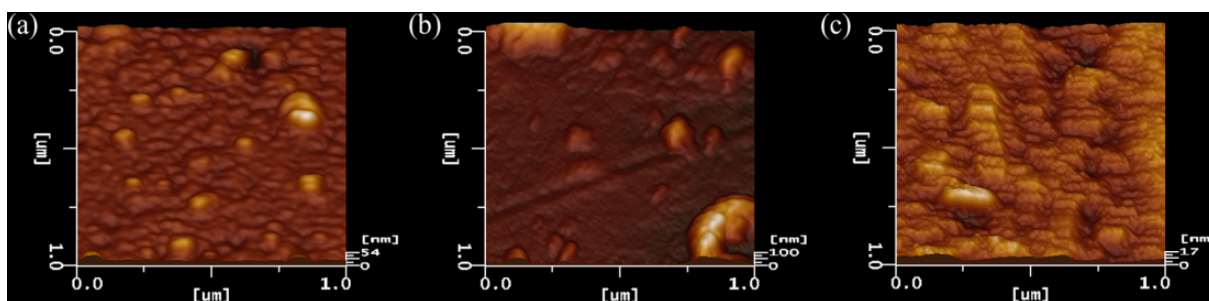
Figure 8. 3-D AFM micrographs (1 × 1 μm) of (a) polymer **3a**, (b) polymer **3b**, and (c) polymer **3c** obtained using **I**. 3-D AFM: three-dimensional atomic force microscopy.

Table 4. Permselectivity coefficients, at 30°C, for different pair of gases in the membranes of **3a**, **3b**, and **3c**, obtained using **I**.

Polymer	α_{O_2/N_2}	α_{CO_2/CH_4}	$\alpha_{C_2O_4/C_3H_6}$	α_{H_2/CH_4}	α_{H_2/C_2H_4}	α_{H_2/C_3H_6}
3a	4.3	23.4	2.3	26.5	16.0	36.3
3b	5.0	26.6	2.1	40.8	27.5	58.1
3c	4.2	21.6	2.0	21.6	14.3	28.7
PPNDI	4.6	21.2	—	20.4	19.0	—

H_2: hydrogen; N_2: nitrogen; O_2: oxygen; CO_2: carbon dioxide; CH_4: methane; C_2H_4: ethylene; C_3H_6: propylene; **3a**: poly(*N*-2-trifluoromethylphenyl-*exo–endo*-norbornen-5,6-dicarboximide); **3b**: poly(*N*-3-trifluoromethylphenyl-*exo–endo*-norbornen-5,6-dicarboximide); **3c**: poly(*N*-4-trifluoromethylphenyl-*exo–endo*-norbornen-5,6-dicarboximide)[13]; PPNDI: poly(*N*-phenyl-*exo–endo*-norbornen-5,6-dicarboximide)[7]; **I**: tricyclohexylphosphine [1,3-bis(2,4,6-trimethylphenyl)-4,5-dihydroimidazol-2-ylidene][benzylidene] ruthenium dichloride.

both. Then, it is possible to factorize the ideal separation factor in two different contributions: a diffusivity selectivity contribution, $a_D = D(A)/D(B)$, and a solubility selectivity contribution, $a_S = S(A)/S(B)$. These will allow us to determine which one of the factors, α_D or α_S makes the larger contribution to attain the gas pair separation.

The comparison of the permselectivities of different pairs of gases in the membranes of **3a**, **3b**, and **3c**, obtained using **I**, is collected in Table 4. As it is seen, the *meta*-substituted polynorbornene dicarboximide **3b** with the lower gas permeability coefficients shows the best ideal separation factors, a trade-off that is commonly found in glassy polymers. In general, the results show that the lower the permeability, the higher the permselectivity. For example, the *ortho* and *para* substitutions of the phenyl group in the parent polymer PPNDI membrane to yield the **3a** and **3c** membranes increase the permeability coefficient of N_2 in 320% and 370%, in slight detriment of the permselectivity coefficient $\alpha(O_2/N_2)$ that decreases about 6% and 9%, respectively. Interestingly, the *meta* substitution of the phenyl group in the parent polymer PPNDI membrane to yield the **3b** membrane not only increases the permeability coefficient of N_2 in 16% but also augments the permselectivity coefficient $\alpha(O_2/N_2)$ nearly 8%, unlike the other substituted polymers. On the other hand, besides exhibiting similar capacities to separate O_2 from N_2 as well as CO_2 from methane (CH_4), in comparison with those of the **3a** and **3c** membranes, the *meta*-substituted **3b** membrane also shows

the highest permselectivity coefficients for separating H_2 from low-molecular-weight hydrocarbon gases such as CH_4, C_2H_4, and propylene (C_3H_6). In fact, these permselectivity coefficients are almost double to those exhibited by the other isomer membranes and are mainly due to an enhancement of the diffusivity selectivity contributions (α_D) that in the case of the pair of gases H_2/C_3H_6 is raised nearly 70% regarding that α_D of the more permeable **3c** membrane for the same pair of gases. In this sense, it is worth noting that $\alpha(H_2/C_3H_6) = 58.1$ for the **3b** membrane is the highest separation factor reported up to now for polynorbornene dicarboximides and the value that best approximate this result ($\alpha(H_2/C_3H_6) = 42.6$) is only obtained by the hydrogenation of the double bonds in this kind of polymers.[10] Furthermore, $\alpha_D = D(H_2)/D(C_3H_6) = 10,420$, for the **3b** membrane, since $\alpha_D >>> \alpha_S$ the diffusivity selectivity makes the larger contribution to attain the gas pair separation. Nevertheless, the low solubility of hydrogen in comparison with that of propylene is responsible for the moderate discriminative properties of the membrane for the separation of hydrogen from propylene.

As mentioned above, the contribution of the solubility process to permselectivity is given by $a_S = S(A)/S(B)$, where A and B are the gases to be separated. An inspection of the values in Table 3 shows that solubility is a poor permselectivity factor for condensable gases. For example, taking propylene as A, in the **3a** membrane, the values of α_S are lower than 3 if B is ethylene and carbon dioxide.
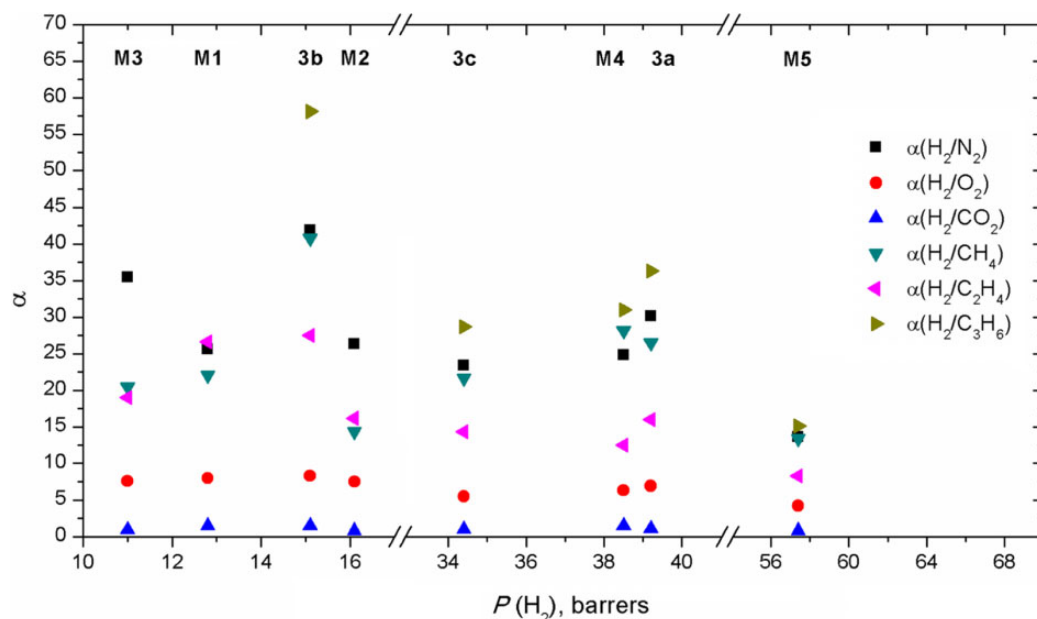
Figure 9. Permselectivity of H_2 with respect to N_2, O_2, CO_2, CH_4, C_2H_4, and C_3H_6 as a function of the permeability of H_2 in the membranes: **3a**, **3b**, **3c**, **M1**, **M2**, **M3**, **M4**, and **M5**. H_2: hydrogen; N_2: nitrogen; O_2: oxygen; CO_2: carbon dioxide; CH_4: methane; C_2H_4: ethylene; C_3H_6: propylene; **3a**: poly(*N*-2-trifluoromethylphenyl-norbornene-5,6-dicarboximide); **3b**: poly(*N*-3-trifluoromethylphenyl-norbornene-5,6-dicarboximide); **3c**: poly(*N*-4-trifluoromethylphenyl-norbornene-5,6-dicarboximide); **M1**: poly(*N*-adamantyl-norbornene-5,6-dicarboximide); **M2**: poly(*N*-cyclohexyl-norbornene-5,6-dicarboximide); **M3**: poly(*N*-phenyl-norbornene-5,6-dicarboximide); **M4**: poly(*N*-pentafluorophenyl-norbornene-5,6-dicarboximide); **M5**: poly(*N*-3,5-bis(trifluoro-methyl)phenyl-norbornene-5,6-dicarboximide).

However, the performance of the selectivity factor is fairly good for the less condensable gases for which α_S may reach values so high as 70, 44, and 17 for N_2, oxygen, and methane, respectively.

Membranes are commonly used to separate hydrogen from both gases and hydrocarbons in petrochemical processes. Then, let us compare briefly the gas separation performances of the membranes **3a**, **3b**, and **3c** with other reported ones having similar chemical structure, in particular, poly(*N*-adamantyl-norbornene-5,6-dicarboximide) (**M1**),[29] poly(*N*-cyclohexyl-norbornene-5,6-dicarboximide) (**M2**),[29] poly(*N*-phenyl-norbornene-5,6-dicarboximide) (**M3**),[29] poly(*N*-pentafluorophenyl-norbornene-5,6-dicarboximide) (**M4**),[7] and poly(*N*-3,5-bis(trifluoro-methyl)phenyl-norbornene-5,6-dicarboximide) (**M5**)[7] regarding the permselectivity of hydrogen with respect to N_2, oxygen, carbon dioxide, CH_4, C_2H_4, and C_3H_6.

Values of $\alpha(H_2/N_2)$, $\alpha(H_2/O_2)$, $\alpha(H_2/CO_2)$, $\alpha(H_2/CH_4)$, $\alpha(H_2/C_2H_4)$, and $\alpha(H_2/C_3H_6)$ are plotted as a function of the permeability coefficient of hydrogen in Figure 9. A correlation between permselectivity and permeability is not clearly seen. Actually, the rule according to which the higher is the permeability the lower is the permselectivity does not seem to hold for $\alpha(H_2/N_2)$ and $\alpha(H_2/CH_4)$ of membrane **3b** when compared with those of the membranes **M3** and **M1**, respectively. In the same sense, the membrane **3c** also displays higher hydrogen permeability and higher

permselectivity for $\alpha(H_2/CH_4)$ in comparison with the membrane **M2**. Pursuing in this line, the membrane **3a** shows higher hydrogen permeability as well as higher permselectivity for $\alpha(H_2/C_3H_6)$, $\alpha(H_2/N_2)$, and $\alpha(H_2/C_2H_4)$ than the fluorinated membrane **M4**. As it is seen in Figure 9, the fluorinated membrane **M5** shows that the higher the permeability the lower the permselectivity, a trade-off that is commonly found in glassy polymers. The values of $\alpha(H_2/O_2)$ and $\alpha(H_2/CO_2)$ are quite similar, and they do not show a clear dependence on the type of membrane. Finally, it is worth noting that membrane **3b** is the most selective to hydrogen with respect to C_3H_6 of all the membranes discussed.

Conclusions

The synthesis and further ROMP of a series of CF_3-bearing polynorbornene dicarboximide isomers were successfully carried out yielding new materials with trifluoromethyl groups systematically located at the *ortho*, *meta*, and *para* position of the aromatic ring attached to the dicarboximide side moiety, respectively. Polymer properties are influenced by the position of the –CF_3 group on the ring mainly due to steric effects. Substitution at the *ortho* position increases the thermomechanical properties of the polymer, whereas *meta* substitution has the opposite effect. The gas transport properties of fluorinated polynorbornenes were

compared to those of the parent unsubstituted polymer. It is observed that the $-CF_3$ group in the *ortho* and *para* positions of the phenyl-substituted polymers increases the permeability of their corresponding membranes as a consequence of the increase of both the gas solubility and the gas diffusion. In contrast, the gas permeability coefficients of the *meta*-substituted membrane are rather similar to those of the non-fluorinated one as a consequence of the decrease of the gas diffusion coefficients attributed to a lower FFV. The *meta*-substituted polymer membrane was also found to have one of the largest permselectivity coefficients reported to date for separating H_2/C_3H_6 in glassy polynorbornene dicarboximides.

Acknowledgments

Declaration of Conflicting Interests

The author(s) declared no potential conflicts of interest with respect to the research, authorship, and/or publication of this article.

Funding

References

1. Li S, Yuan J, Deng P, et al. Synthesis and photovoltaic properties of new conjugated polymers based on two angular-shaped naphthodifuran isomers and isoindigo. *Sol Energy Mat Sol Cells* 2013; **118**: 22–29.

2. Zhao B, Sun K, Xue F, et al. Isomers of dialkyl diketopyrrolo-pyrrole: electron-deficient units for organic semiconductors. *Org Electron* 2012; **13**: 2516–2524.

3. Zhou CZ, Wanga WL, Linb KK, et al. Poly(naphthylenethiophene)s and poly(naphthylenevinylenephenylenevinylene)s: effect of naphthalene positional isomers on the light emitting properties of their polymers. *Polymer* 2004; **45**: 2271–2279.

4. Yampolskii Y, Pinnau I and Freeman BD. Transport of gases and vapors in glassy and rubbery polymers, Section 1.5 structure / properties relations. In Yampolskii Y (ed) *Materials science of membranes for gas and vapor separation*. England: John Wiley & Sons Ltd, 2006, p. 159. DOI: 10.1002/047002903X, ISBN: 978-0-470-85345-0

5. Song Y, Jin Y, Yang T, et al. Structure–property studies on fluorinated polyimide isomers containing biphenyl moieties. *High Perform Polym* 2012; **24**: 488–494.

6. Kim S, Seong JG, Do YS, et al. Gas sorption and transport in thermally rearranged polybenzoxazole membranes derived from polyhydroxylamides. *J Membr Sci* 2015; **474**: 122–131.

7. Vargas J, Santiago AA, Tlenkopatchev MA, et al. Gas transport in membranes based on polynorbornenes with fluorinated dicarboximide side moieties. *J Membr Sci* 2010; **361**: 78–88.

8. Vargas J, Martínez A, Santiago AA, et al. Synthesis and gas permeability of new polynorbornene dicarboximide with fluorine pendant groups. *Polymer* 2007; **48**: 6546–6553.

9. Yampolskii Y. Polymeric gas separation membranes. *Macromolecules* 2012; **45**: 3298–3311.

10. Vargas J, Santiago AA, Cruz-Morales JA, et al. Gas transport properties of hydrogenated and fluorinated polynorbornene dicarboximides. *Macromol Chem Phys* 2013; **214**: 2607–2615.

11. Vargas J, Santiago AA, Tlenkopatchev MA, et al. Gas transport in polymers prepared via metathesis copolymerization of *exo-N*-phenyl-7-oxanorbornene-5,6-dicarboximide and norbornene. *Macromolecules* 2007; **40**: 563–570.

12. Martínez A, Clark-Tapia R, Gutiérrez S, et al. Synthesis and characterization of new ruthenium vinylidene complexes. *Lett Org Chem* 2014; **11**: 748–754.

13. Vargas J, Martínez A, Santiago AA, et al. The effect of fluorine atoms on gas transport properties of new polynorbornene dicarboximides. *J Fluorine Chem* 2009; **130**: 162–168.

14. Barrer RM. Permeation, diffusion and solution of gases in organic polymers. *Trans Faraday Soc* 1939; **35**: 628–643.

15. Santiago AA, Vargas J, Tlenkopatchev MA, et al. Electrochemical performance of membranes based on hydrogenated polynorbornenes functionalized with imide side groups containing sulfonated fluorinated moieties. *J Mem Sci* 2012; **403-404**: 121–128.

16. Santiago AA, Vargas J, Fomine S, et al. Polynorbornene with pentafluorophenyl imide side chain groups: Synthesis and sulfonation *J Polym Sci A: Polym Chem* 2010; **48**: 2925–2933.

17. Sanford MS, Ulman M and Grubbs RH. New insights into the mechanism of ruthenium-catalyzed olefin metathesis reactions. *J Am Chem Soc* 2001; **123**: 749–750.

18. Fomine S, Vargas SM and Tlenkopatchev MA. Molecular modeling of ruthenium alkylidene mediated olefin metathesis reactions. DFT study of reaction pathways *Organometallics* 2003; **22**: 93–99.

19. Fomine S and Tlenkopatchev MA. Metathesis of fluorinated olefins by ruthenium alkylidene catalysts. Fluorine substituent effects on a Ru-carbene (alkylidene) complex stability: a computational study. *Appl Catal, A* 2009; **355**: 148–155.

20. Asrar J. High-temperature metathesis polymers: Structure-property relationships *Macromolecules* 1994; **27**: 4036–4042.

21. Garbow JR, Goetz J and Asrar J. Polymers of methyl-substituted *n*-phenylnorbornene-5,6-dicarboximide: characterization of structure and dynamics. *Macromolecule*s 1998; **31**: 3925–3930.

22. Bondi A. *Physical properties of molecular crystals, liquids and glasses*. 2nd ed. New York: John Wiley & Sons Ltd, 1968, pp. 370–439.

23. Van Krevelen DW. *Properties of polymers, their correlation with chemical structure; estimation and prediction from additive group contributions*. 4th ed. United Kingdom: Elsevier Science Publishers, 2009, p. 655. ISBN: 978-0-08-054819-7

24. Santiago AA, Vargas J, Cruz-Gómez J, et al. Synthesis and ionic transport of sulfonated ring-opened polynorbornene based copolymers. *Polymer* 2011; **52**: 4208–4220.

25. Charati SG, Houde AY, Kulkarni SS, et al. Transport of gases in aromatic polyesters: Correlation with WAXD studies. *J Polym Sci, B: Polym Phys* 1991; **29**: 921–931.

26. Constantin C-P, Damaceanu M-D, Varganici C, et al. Dielectric and gas transport properties of highly fluorinated polyimides blends. *High Perform Polym* 2015; **27**: 526–538.

27. Eguchi H, Kim DJ and Koros WJ. Chemically cross-linkable polyimide membranes for improved transport plasticization resistance for natural gas separation. *Polymer* 2015; **58**: 121–129.

28. Kanehashi S and Nagai K. Analysis of dual-mode model parameters for gas sorption in glassy polymers. *J Membr Sci* 2005; **253**: 117–138.

29. Contreras AP, Tlenkopatchev MA, López-González MM, et al. Synthesis and gas transport properties of new high glass transition temperature ring-opened polynorbornenes. *Macromolecules* 2002; **35**: 4677–4684.